Coupled Electronic States in *trans*-Dioxo Complexes of Rhenium(V) and Osmium(VI) Probed by Near-Infrared and Visible Luminescence Spectroscopy

Carole Savoie and Christian Reber*

Contribution from the Département de chimie, Université de Montréal, Montréal QC H3C 3J7, Canada

Received September 13, 1999

Abstract: *trans*-Dioxo complexes of rhenium(V) and osmium(VI) with ethylenediamine, imidazole, and oxalate ancillary ligands show luminescence maxima varying between 620 and 900 nm. The resolved vibronic progressions of the rhenium complexes have intensity distributions that cannot be rationalized with harmonic potential energy surfaces. The broadband spectra of the osmium(VI) complexes also show deviations from the band shapes expected for a harmonic ground-state potential surface. We use the large variation of luminescence energies and the vibronic features to show the influence of excited electronic states on the ground-state potential energy surface. The vibronic structure and band envelopes of the luminescence spectra are calculated using the lowest energy adiabatic surface obtained from three interacting electronic states.

Introduction

The excited electronic states of a molecule are generally not considered to have a significant influence on its ground state properties, because they are well separated in energy from the ground state. We use a series of transition metal complexes to show that excited states in the visible and near-infrared spectral region do influence the ground state potential energy surface. Dramatic spectroscopic effects have previously been reported to arise from coupled excited states of transition metal compounds, leading to intensity borrowing,[1] interference dips,[2] or unusual spacings of resolved vibronic progressions,[3] observations which have been rationalized in a consistent way with time dependent quantum mechanical models based on coupled potential energy surfaces.[4] We use this theoretical approach in the following, but apply it to the study of *ground state* properties of *trans*-dioxo complexes of rhenium(V) and osmium(VI), a class of compounds whose photochemical and electrochemical properties have received considerable interest.[5−12]

The influence of the excited states on the ground-state potential surface is experimentally determined from low-temperature luminescence spectra of crystalline *trans*-dioxo complexes. The importance of interactions between electronic states for situations other than the well-studied Jahn−Teller[13,14] or intervalence electron-transfer potentials[15,16] has traditionally been neglected in the analysis and understanding of spectra and properties of transition metal compounds. Several recent reviews focus on such effects from a theoretical perspective and include detailed analyses of the dynamics for model systems such as diatomic and triatomic molecules.[17,18] The photochemical consequences of coupled excited states for organic reactions have also been reviewed recently.[19] We attempt to transfer some of these approaches to transition metal chemistry, which often involves molecules that are too complicated to be studied by full theoretical analyses. The title complexes allow us to benefit as much as possible from symmetry and different types of metal−ligand bonds.

We examine a series of *trans*-dioxo complexes of rhenium(V) and osmium(VI) with the $[Xe]5d^2$ electron configuration and ethylenediamine, vinylimidazole, and carboxylate ancillary ligands, abbreviated as L in the following. These molecules show luminescence that can be tuned over a wide energy range through the use of different ancillary ligands. Their absorption and vibrational spectra are well studied, but their luminescence spectroscopy has received less attention, with the exception of *trans*-$ReO_2(pyridine)_4^+$, a complex with a luminescence maximum at 650 nm and resolved vibronic structure,[5,6] and a series of *trans*-dioxo complexes of osmium(VI) with cyanide or macrocyclic nitrogen donor ligands, which show luminescence maxima between 620 nm[10] and 700 nm.[9,20] We present and analyze previously unreported luminescence data for six *trans*-dioxo complexes.

The ground state of all title compounds has no orbital or spin degeneracy, an important prerequisite to observe subtle vibronic effects which are easily hidden in spectra consisting of a

* Address correspondence to this author.

(1) Wexler, D.; Zink, J. I.; Reber, C. *J. Phys. Chem.* **1992**, *96*, 8757.
(2) Reber, C.; Zink, J. I. *J. Chem. Phys.* **1992**, *96*, 2681.
(3) Bussière, G.; Reber, C. *J. Am.. Chem. Soc.* **1998**, *120*, 6306.
(4) Reber, C.; Zink, J. I. *Comm. Inorg. Chem.* **1992**, *13*, 177.
(5) Winkler, J. R.; Gray, H. B. *J. Am. Chem. Soc.* **1983**, *105*, 1373.
(6) Winkler, J. R.; Gray, H. B. *Inorg. Chem.* **1985**, *24*, 346.
(7) Thorp, H. H.; Kumer, C. V.; Turro, N. J.; Gray, H. B. *J. Am. Chem. Soc.* **1989**, *111*, 4364.
(8) Thorp, H. H.; Van Houten, J.; Gray, H. B. *Inorg. Chem.* **1989**, *28*, 889.
(9) Che, C.-M.; Yam, V. W.-W.; Cho, K.-C.; Gray, H. B. *J. Chem. Soc. Chem. Commun.* **1987**, 948.
(10) Che, C.-M.; Cheng, W.-K.; Yam, V. W.-W. *J. Chem. Soc., Dalton Trans.* **1990**, 3095.
(11) Schindler, S.; Castner, E. W., Jr.; Creutz, C.; Sutin, N. *Inorg. Chem.* **1993**, *32*, 4200.
(12) Creutz, C.; Chou, M. H. *Inorg. Chem.* **1994**, *33*, 3199.
(13) Sturge, M. D. *Solid State Phys.* **1967**, *20*, 91.
(14) Sturge, M. D. *Phys. Rev. B* **1970**, *1*, 1005.
(15) *Mixed-Valence Compounds*; Brown, D. B., Ed.; Reidel: Dordrecht, 1980.
(16) Talaga, D. S.; Zink, J. I. *J. Phys. Chem.* **1996**, *100*, 8712.
(17) Romstad, D.; Granucci, G.; Persico, M. *Chem. Phys.* **1997**, *219*, 21.
(18) Butler, L. J. *Annu. Rev. Phys. Chem.* **1998**, *49*, 125.
(19) Bernardi, F.; Olivucci, M.; Robb, M. A. *Chem. Soc. Rev.* **1996**, 322.
(20) Sartori, C.; Preetz, W. *Z. Naturforsch.* **1988**, *43a*, 239.

10.1021/ja993305q CCC: $19.00
Published on Web 01/20/2000

superposition of transitions to final states arising from a degenerate ground-state split by spin−orbit coupling or low symmetry. The high symmetry allows us to apply crystal field theory to define the energies and metal−ligand bonding characteristics of the relevant excited states. The single and double metal−ligand bonds have well separated vibrational frequencies and normal coordinates that involve predominantly only one type of ligand, an important advantage for the analysis of the vibronic structure of the luminescence spectra. Metal−oxo vibrational frequencies are higher than metal−ancillary ligand frequencies by approximately a factor of 4 and both modes are therefore easily identified in the vibronic structure of an electronic spectrum. A recent quantitative normal coordinate analysis of *trans*-$OsO_2(oxalate)_2^{2-}$ and *trans*-$OsO_2(malonate)_2^{2-}$ [21] concludes that the Os═O oscillators contribute between 98% and 100% to the metal−oxo coordinate and that the metal−ligand modes involving the ancillary ligands L have between 39% and 48% metal−L character, with the remaining contributions originating from oscillators centered on L.

We find that not only the lowest energy excited state influences the potential energy surface of the ground state. A model involving two excited states is necessary to calculate the vibronic structure of the luminescence spectra for our series of related molecules. Low-temperature optical spectroscopy provides a powerful approach to characterize interactions between electronic states, information not easily available from other experimental or theoretical techniques. We have applied absorption spectroscopy in a previous study[3] and use luminescence spectroscopy in the following.

Experimental Section

All *trans*-dioxo complexes of rhenium(V) were prepared using literature methods.[22−26] Both *trans*-$ReO_2(ethylenediamine)_2Cl$ and *trans*-$ReO_2(N,N,N',N'$-tetramethylethylenediamine$)_2Cl$ were prepared from solutions of $ReOCl_2(OEt)(PPh_3)_2$[22] in absolute ethanol, to which an excess of the ethylenediamine ligand was added.[6] After 1 h at reflux a yellow solid precipitated, which then was recrystallized several times from a methanol/water 1:1 mixture. *trans*-$ReO_2(1$-vinylimidazole$)_4I$ was prepared by adding an excess of the ligand to a suspension of $ReO_2I(PPh_3)_2$[27] in methanol. The crystals obtained were filtered and washed with toluene. Both *trans*-$OsO_2(en)_2Cl_2$ and *trans*-$OsO_2(oxalate)_2(NBu_4)_2$ were prepared according to literature methods[28,29] from $K_2OsO_4{\cdot}2H_2O$ (Strem Chemicals) and recrystallized from ethanol/ether. The ancillary ligands ethylenediamine, *N,N,N′,N′*-tetramethylethylenediamine, 1-vinylimidazole, and oxalate will be abbreviated as en, tmen, vi-im, and ox in the following and we will use only the formula of the transition metal complex without the counterion for brevity. The purity of all compounds was checked by IR, Raman, and electronic spectroscopy.

The luminescence instrumentation has been described in detail before.[30] A Xe lamp filtered through a copper sulfate solution and Schott BG18 or UG11 filters was used as excitation source. The samples were cooled in a helium gas-flow cryostat (Oxford Instruments CF 1204). The emitted light was dispersed through a 0.75 m monochromator (Spex 1800 II) or a 0.5 m monochromator (Spex 500M) and detected with photomultipliers (Hamamatsu R4632, R928 or R406) or a Ge near-infrared detector (Applied Detector Corporation 403UL). All luminescence spectra were corrected for detector response by calibration with a calibrated reference tungsten lamp (Oriel 63350), using the procedure described in detail previously.[30]

Luminescence lifetimes were measured with an excimer laser (XeCl, 308 nm) as excitation source and detected with a Hamamatsu R406 photomultiplier. The time-dependent intensities were stored with a digital oscilloscope (Tektronix TDS380).[31] Absorption spectra were measured with a Varian Cary 5E spectrometer.

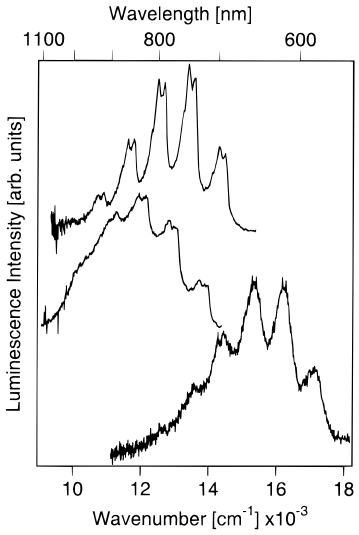

Figure 1. Solid-state luminescence spectra of *trans*-$ReO_2(tmen)_2Cl$ (10 K, bottom trace), *trans*-$ReO_2(en)_2Cl$ (15 K, middle trace), and *trans*-$ReO_2(1$-vinylimidazole$)_4I$ (6 K, top trace).

Table 1. Summary of Spectroscopic Data from Low-temperature Crystal Spectra of *trans*-Dioxo Complexes

complex	lum. max. [cm^{-1}]	lum. origin [cm^{-1}]	lum. lifetime [μs]	$\hbar\omega_{M=O}$ [cm^{-1}]	$\hbar\omega_{M-L}$ [cm^{-1}]
$ReO_2(en)_2^+$	12190	14200	1.6 (10 K) 1.0 (80 K)	880[a] 899[b] 795[c]	210[a] 260[c]
$ReO_2(tmen)_2^+$	15910	17660	62 (10 K) 60 (100 K) 42 (250 K)	890[a]	200[a]
$ReO_2(vi\text{-}im)_4^+$	13310	14700		885[a]	175[a] 210[c]
$OsO_2(en)_2^{2+}$	13550	15200	0.89 (10 K) 0.82 (100 K) 0.40 (250 K)	912[b] 726[c]	236[b] 270[b]
$OsO_2(ox)_2^{2-}$	11050[e]	12600	0.36 (16 K) 0.32 (80 K) 0.20 (120 K)	907[d] 910[d] 730[c]	561[d] 569[d]

[a] Luminescence. [b] Raman. [c] Absorption (^3E_g excited state). [d] Raman, refs 20 and 21. [e] *trans*-$OsO_2(malonate)_2^{2-}$ shows a weak luminescence band with a maximum at 10600 cm^{-1} (10 K).

Spectroscopic Results

Crystals of all *trans*-dioxo complexes used for this study show luminescence at low temperatures. The spectra of *trans*-$ReO_2(vi\text{-}im)_4^+$, *trans*-$ReO_2(en)_2^+$, and *trans*-$ReO_2(tmen)_2^+$ are presented in Figure 1. It is remarkable that these closely related complexes show band maxima separated by 3700 cm^{-1}. The luminescence spectra in Figure 1 show a main progression with an average spacing of 900 cm^{-1}. The comparison of this energy difference with Raman frequencies is given in Table 1 for all complexes, confirming that this progression involves the Raman active rhenium−oxo stretching mode. The overall band enve-

(21) Struess, A.; Preetz, W. *Z. Naturforsch.* **1998**, *53b*, 823.
(22) Chatt, J.; Rowe, G. A. *J. Chem. Soc.* **1962**, 4019.
(23) Johnson, N. P.; Lock, C. J. L.; Wilkinson, G. *J. Chem. Soc.* **1964**, 1054.
(24) Lock, C. J. L.; Turner, G. *Acta Crystallogr.* **1978**, *B34*, 923.
(25) Brewer, J. C.; Gray, H. B. *Inorg. Chem.* **1989**, *28*, 3334.
(26) Bélanger, S.; Beauchamp, A. L. *Inorg. Chem.* **1996**, *35*, 7836.
(27) Ciani, G. F.; D'Alfonso, G.; Romiti, P. F.; Sironi, A.; Freni, M. *Inorg. Chim. Acta* **1983**, *72*, 29.
(28) Malin, J. M.; Schlemper, E. O.; Murmann, R. K. *Inorg. Chem.* **1977**, *16*, 615.
(29) Preetz, W.; Schulz, H. *Z. Naturforsch.* **1983**, *38b*, 183.
(30) Davis, M. J.; Reber, C. *Inorg. Chem.* **1995**, *34*, 4585.
(31) Weiss, J.; Fischer, R. A.; Pelletier, Y.; Reber, C. *Inorg. Chem.* **1998**, *37*, 3316.

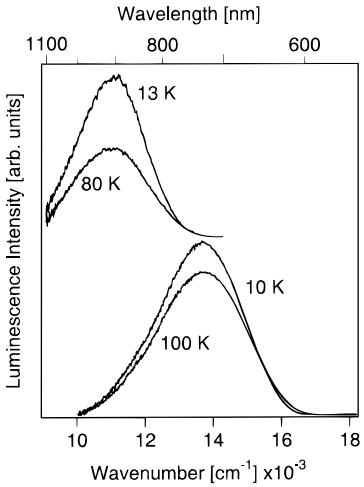

Figure 2. Solid-state luminescence spectra of *trans*-$OsO_2(en)_2Cl_2$ (10 and 100 K, bottom traces) and *trans*-$OsO_2(ox)_2(NBu_4)_2$ (13 and 80 K, top traces). The abscissa scale is identical with that in Figure 1.

lopes and intensity distribution along the main progression of the spectra in Figure 1 are similar to the literature spectrum of *trans*-$ReO_2(pyridine)_4^+$ [5,6] and to the spectra of seven *trans*-$ReO_2(R\text{-imidazole})_4^+$ complexes with different substituents R on the ligand ring system.[32] Each member of the main progression consists of a cluster of bands separated by approximately 200 cm^{-1}, particularly obvious for *trans*-$ReO_2(en)_2^+$ and *trans*-$ReO_2(vi\text{-}im)_4^+$ in Figure 1. These energy differences are in good agreement with low-frequency Raman transitions involving predominantly metal−L oscillators. Our low-temperature absorption spectrum of *trans*-$ReO_2(en)_2^+$ is identical with the literature.[6] The lowest-energy absorption bands of *trans*-$ReO_2(tmen)_2^+$ are approximately 4000 cm^{-1} higher in energy than those of the ethylenediamine complex. The absorption spectra of both compounds overlap with the luminescence spectra at the electronic origin.

Luminescence lifetimes and intensities show similar decreases at high temperatures and are given at representative temperatures in Table 1. The luminescence lifetime of $ReO_2(tmen)_2^+$ is 62 μs at 10 K, similar to the 68 μs lifetime reported at low temperature for $ReO_2(pyridine)_4^+$ [6] and longer by a factor of 50 than the 1.6 μs lifetime of $ReO_2(en)_2^+$ at 10 K. This difference is most likely due to more efficient nonradiative relaxation processes for complexes with low energy emission bands, such as $ReO_2(en)_2^+$. Similar lifetimes between 1 and 3 μs have been determined before for a series of *trans*-$ReO_2(R\text{-imidazole})_4^+$ complexes with emissions in the near-infrared spectral region.[32]

Figure 2 shows the luminescence spectra of *trans*-$OsO_2(ox)_2^{2-}$ and *trans*-$OsO_2(en)_2^{2+}$. Both spectra have no resolved vibronic structure. The band maxima of the two complexes are separated by 2500 cm^{-1}, an energy variation comparable to the value determined for the rhenium complexes in Figure 1. The full luminescence bandwidths at half-height are 3150 and 2380 cm^{-1} for *trans*-$OsO_2(en)_2^{2+}$ and *trans*-$OsO_2(ox)_2^{2-}$, respectively. The absorption spectrum of *trans*-$OsO_2(ox)_2^{2-}$ is given in the literature[29,33] and shows the onset of a weak band system in the same energy region as the high-energy limit of the luminescence spectrum at approximately 14000 cm^{-1} in Figure 2. The absorption spectrum of *trans*-$OsO_2(en)_2^{2+}$ also shows weak, structured bands starting at approximately 18000 cm^{-1}, coinciding with the high-energy limit of the luminescence band. The average spacing of the main progression in the absorption spectrum is 726 cm^{-1}. At 26810 and 31250 cm^{-1} the origins of two intense oxo → osmium(VI) charge-transfer bands are observed. Their vibronic structure and widths are similar to those reported and analyzed for many other *trans*-dioxo complexes of osmium(VI), independent of the nature of their ancillary ligands.[9−12,20,29,33] The luminescence intensity of both *trans*-dioxo osmium(VI) complexes decreases at high temperatures, as illustrated with the high-temperature spectra included in Figure 2. The luminescence lifetime of *trans*-$OsO_2(en)_2^{2+}$ is 0.89 μs at 10 K, significantly longer than the lifetime of 0.36 μs measured at 13 K for *trans*-$OsO_2(ox)_2^{2-}$, which emits at lower energy. The luminescence lifetime for *trans*-$OsO_2(ox)_2^{2-}$ varies by only 9 ns between 840 and 940 nm, indicating that the observed unresolved band is not a superposition of individual spectra from significantly different chromophores. Table 1 contains a summary of the relevant spectroscopic data for all *trans*-dioxo complexes compared in the following.

Discussion

Totally Symmetric Electronic States of *trans*-Dioxo Complexes. In this section, we identify excited electronic states with the same symmetry as the ground state and define a model for the ground-state potential energy surface that includes interactions with the excited states. The d-orbitals of a *trans*-dioxo complex with D_{4h} point group symmetry and the *z* axis parallel to the metal−oxo bond split into b_{2g} (d_{xy}), e_g ($d_{xz,yz}$), b_{1g} ($d_{x^2-y^2}$), and a_{1g} (d_{z^2}) in increasing order of energy.[6,34] We will only consider electronic states arising from $(b_{2g})^n(e_g)^m$ orbital configurations (n, m: 0, 1, 2; $n + m = 2$). The ground state of all *trans*-dioxo compounds studied here is $^1A_{1g}$ and arises from the $(b_{2g})^2$ electron configuration. Spin−orbit coupling is an important effect in complexes of third-row transition metals, and we will therefore use interactions between spin−orbit states of A_{1g} symmetry. Their spin and orbit symmetry and electron configurations are given in Figure 3. The lowest-energy excited A_{1g} state is a spin−orbit level of the ^3E_g crystal field state with the $(b_{2g})(e_g)$ electron configuration. It is not the emitting state, as the B_{1g} and B_{2g} spin−orbit levels are lower in energy for all title complexes.[6,34] The second A_{1g} excited state within our model is the $^1A_{1g}$ state arising from the $(e_g)^2$ electron configuration.[34] These three states interact through off-diagonal matrix elements involving spin−orbit coupling and interelectronic repulsion. Their electronic energies are obtained as eigenvalues of:

$$V_{A_{1g}} = \begin{pmatrix} E_1 & V_{12} & V_{13} \\ V_{12} & E_2 & V_{23} \\ V_{13} & V_{23} & E_3 \end{pmatrix} \quad (1)$$

The diagonal elements E_i are given in the literature[34] in terms of crystal field theory (CF) using the angular overlap formalism:

$$E_1^{CF} = E(^1A_{1g}, b_{2g}^2) = 3K_{xy} = 3(3B + C) \quad (2)$$

$$E_2^{CF} = E(^3E_g, b_{2g}e_g) = \Delta_\pi = 2(e_\pi(O) - e_\pi(L)) \quad (3)$$

$$E_3^{CF} = E(^1A_{1g}, e_g^2) = 2\Delta_\pi + 4K_{xy} \quad (4)$$

Empirical values for the two crystal field parameters Δ_π and

(32) Savoie, C.; Reber, C. *Coord. Chem. Rev.* **1998**, *171*, 387.
(33) Cromp, B.; Triest, M.; Carrington, T., Jr.; Reber, C. *Spectrochim. Acta A* **1999**, *55*, 575.
(34) Miskowski, V. M.; Gray, H. B.; Hopkins, M. D. In *Advances in Transition Metal Coordination Chemistry*; Che, C.-M., Yam, V. W.-W., Eds.; JAI Press: Greenwich, CT, 1996; Vol. 1, p 159.

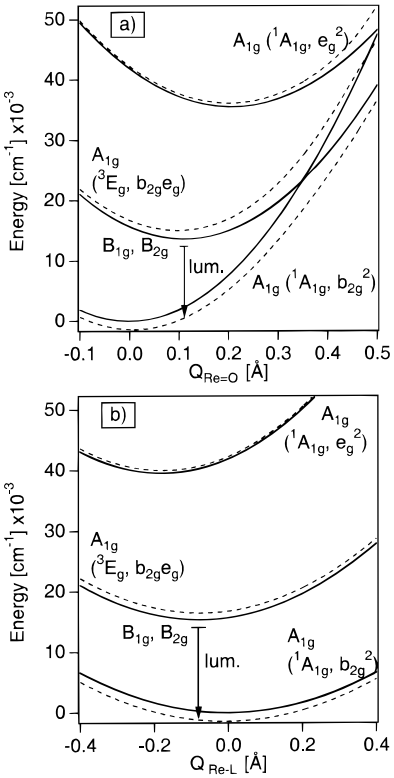

Figure 3. Potential energy surfaces for *trans*-ReO_2(1-vinylimidazole)$_4^+$ along the rhenium−oxo (a) and rhenium−(1-vinylimidazole) (b) normal coordinates. Electronic states are indicated in idealized D_{4h} symmetry and their orbital configurations are given. Adiabatic potential energy surfaces that include coupling between electronic states are given as dotted lines, as calculated from eq 1. The arrow denotes the luminescence transition from the lowest energy spin−orbit levels of the ^3E_g excited state to the $^1A_{1g}$ ground state. The parity forbidden transition is allowed by the low actual symmetry of the compound and by vibronic mechanisms.

K_{xy} are given in the literature.[34] The parameter Δ_π has been determined to be on the order of 24800 cm^{-1} for saturated nitrogen donor ancillary ligands and values between 1800 and 2400 cm^{-1} have been reported for K_{xy}.[34] These two parameters are the most important factors determining the luminescence energies and the energies of the three electronic states in eq 1. We have shown previously with molecular orbital and crystal field calculations that *trans*-ReO_2(R-imidazole)$_4^+$ complexes have lower Δ_π values than *trans*-$ReO_2(py)_4^+$ and luminesce therefore at significantly lower energy.[32] The decrease of K_{xy} from *trans*-$ReO_2(en)_2^+$ to *trans*-$ReO_2(tmen)_2^+$ leads to the different luminescence energies for these two complexes, as illustrated in Figure 1.[32] Significant decreases of the Racah parameters for complexes with substituted ethylenediamine ligands with respect to their ethylenediamine analogues have been reported for tetragonal *trans*-Ni(SCN)$(en)_2$ complexes,[35,36] confirming the trend observed for *trans*-$ReO_2L_2^+$ complexes.

We use angular overlap calculations[37] including spin−orbit coupling within the $5d^2$ configuration to calculate the crystal field energy differences between two A_{1g} excited states and the ground state. These energy differences are given as $E_{calc}(A_{1g},{}^3E_g)$ and $E_{calc}(A_{1g},{}^1A_{1g})$ in Table 2. The off-diagonal matrix elements V_{12}, V_{13}, and V_{23} are adjusted by fitting the eigenvalues of eq 1 to the crystal field energies of the three A_{1g} states. This procedure allows us to include effects arising from coupling to all A_{1g} electronic states and can easily be simplified to a two-state model by considering only the upper left-hand 2×2 matrix of eq 1. The matrix element between the two $^1A_{1g}$ electronic states is given as $\sqrt{2}K_{xy}$[34] and the matrix element between the ground state and the lowest energy A_{1g} excited state is expected to be on the order of the spin−orbit coupling constant ζ. The numerical values of V_{ij} in Table 2 are in this range and will be used to calculate the effects of the two excited states on the ground-state potential surface. The off-diagonal matrix elements are treated as constants in the following. The diagonal elements correspond to harmonic potential energy surfaces with vibrational frequencies and positions of their minima along the normal coordinate axes determined from luminescence, absorption, and Raman spectra.

Calculation of Luminescence Spectra. The matrix in eq 1 represents the energies of the three A_{1g} electronic states at the ground-state equilibrium geometry and the values of E_1, E_2, and E_3 given by eqs 2−4 do not vary as a function of molecular structure. It is essential to realize that the energy minima of the excited states correspond to molecular structures that are different from the ground-state equilibrium geometry. E_1, E_2, and E_3 represent therefore potential energy surfaces in a model that allows us to calculate spectra. We use the harmonic potential surfaces given in eqs 5−7 as a function of the metal−oxo ($Q_{M=O}$) and metal−L (Q_{M-L}) normal coordinates.

$$E_1 = E_1^{CF} + \frac{k_{M=O}}{2}Q_{M=O}^2 + \frac{k_{M-L}}{2}Q_{M-L}^2 \quad (5)$$

$$E_2 = E_2^{CF} + \frac{k'_{M=O}}{2}(Q_{M=O}^2 - 2Q_{M=O}\Delta Q_{M=O}) + \frac{k'_{M-L}}{2}(Q_{M-L}^2 - 2Q_{M-L}\Delta Q_{M-L}) \quad (6)$$

$$E_3 = E_3^{CF} + \frac{k'^2_{M=O}}{2k_{M=O}}(Q_{M=O}^2 - 4Q_{M=O}\Delta Q_{M=O}) + \frac{k'^2_{M-L}}{2k_{M-L}}(Q_{M-L}^2 - 4Q_{M-L}\Delta Q_{M-L}) \quad (7)$$

The force constants k_i in eqs 5−7 are calculated from the experimental vibrational frequencies in Table 1. The energy $E_{calc}(A_{1g},{}^3E_g)$ obtained from the crystal field calculation compares favorably to the first absorption maxima of the rhenium complexes. The potential minima for both excited states E_2 and E_3 are defined by $\Delta Q_{M=O}$ and ΔQ_{M-L}. These two parameters are obtained from the comparison of calculated and experimental luminescence and absorption spectra. Metal−oxo bond length changes are obtained as $\Delta Q_{M=O}/\sqrt{2}$. The orbital configurations of the two lowest energy electronic states and the ground and excited-state vibrational frequencies in Table 1 define the signs of these bond length changes. The excitation of a molecule to its $A_{1g}(^3E_g)$ excited state (E_2) increases electron density in the π antibonding e_g orbitals oriented toward the oxo ligands. The metal−oxo vibrational energy of this excited state decreases to approximately 90% of the ground-state value, and we expect the bond length to increase. The values of $\Delta Q_{M=O}$ given in Table 2 are similar for all complexes, reflecting their almost identical metal−oxo bonding. In the $A_{1g}(^3E_g)$ excited state electron density is removed from the π antibonding b_{2g} orbital oriented

(35) Lever, A. B. P.; London, G.; McCarthy, P. J. *Can. J. Chem.* **1977**, *55*, 3172.

(36) Lever, A. B. P.; Walker, I. M.; McCarthy, P. J.; Mertes, K. B.; Jircitano, A.; Sheldon, R. *Inorg. Chem.* **1983**, *22*, 2252.

(37) Adamsky, H. *AOMX − an angular overlap program*; Institut für Theoretische Chemie, Heinrich-Heine-Universität Düsseldorf: Düsseldorf, Germany, 1995. The program is available at http://www.theochem.uni-duesseldorf.de/Computing/Progs/aomx/Welcome.html.

Table 2. Summary of Parameters for the Calculation of Spectra of *trans*-Dioxo Complexes

	$ReO_2(vi\text{-}im)_4^+$	$ReO_2(en)_2^+$	$ReO_2(tmen)_2^+$	$OsO_2(ox)_2^{2-}$	$OsO_2(en)_2^{2+}$
Δ_π [cm^{-1}]	10970	22000	22000		
K_{xy} [cm^{-1}]	2000	3100	2000		
ζ [cm^{-1}]	3000	3000	3000		
V_{12} [cm^{-1}]	2160	420	2250	4000	0
V_{13} [cm^{-1}]	2690	441	2980		
V_{23} [cm^{-1}]	4600	4620	4820		
$E_{calc}(A_{1g},{}^3E_g)$ [cm^{-1}]	15670	15700	18490		
$E_{calc}(A_{1g},{}^1A_{1g})$ [cm^{-1}]	41890	48560	47860		
$\Delta Q_{M=O}$ [Å]	0.11	0.13	0.12	0.085	0.10
ΔQ_{M-L} [Å]	−0.08	−0.11	−0.08		
Γ [cm^{-1}]	50	50	50	350	350

toward the ancillary ligands, and the M−L vibrational frequency of the excited state increases to 120% of the ground-state value, leading to a bond length decrease and to the negative values of ΔQ_{M-L} in Table 2.

The highest energy A_{1g} state ($^1A_{1g}$, e_g^2 configuration) cannot be observed spectroscopically, but it can be characterized with eqs 1−5 and with reasonable estimates for its force constant and for the position of its potential minimum along the coordinates Q_i. We assume in eq 7 that its ΔQ_i values correspond to the double of those obtained for the $A_{1g}(^3E_g)$ state, where only one electron is excited into the e_g orbital. We estimate vibrational frequencies that change by a factor of k_2/k_1 from the values obtained for the $A_{1g}(^3E_g)$ excited state. Figure 3 shows the harmonic potentials in eqs 5−7 as a function of both relevant normal coordinates. The excited-state potentials cause a flattening of the ground-state surface at positive values of $Q_{Re=O}$ and negative values of Q_{M-L}. The higher energy excited state in eq 1 effectively represents both high-energy crystal field states or totally symmetric charge transfer states. Qualitative experimental evidence for this excited state is observed in the absorption spectrum of *trans*-$ReO_2(en)_2^+$, which shows a weak band with a resolved progression in the Re=O mode starting at approximately 28000 cm^{-1}, possibly corresponding to the second excited state in our model and confirming our assumption of a large offset of its potential energy minimum along $Q_{Re=O}$. In other compounds, this transition is masked by more intense transitions to ungerade parity excited states. The contour lines in Figure 4a show the potential surface for a harmonic ground state, calculated from eq 1 with $V_{12} = V_{13} = V_{23} = 0$. The contour diagram in Figure 4b is calculated for the lowest energy adiabatic surface obtained from eq 1 with the nonzero coupling constants V_{ij} given in Table 2 for *trans*-$ReO_2(vi\text{-}im)_4^+$, again illustrating the flattening caused by the excited electronic states.

The analytical expression for the ground-state potential surface, corresponding to the lowest-energy eigenvalue of eq 1 with the diagonal elements of the matrix given by eqs 5−7, contains many terms of the form $k_c Q_{M=O}{}^m Q_{M-L}{}^n$ ($m + n \leq 6$, $m \neq 0$, $n \neq 0$). These terms lead to potential energy surfaces such as Figure 4b where the $Q_{M=O}$ and Q_{M-L} coordinates can no longer be separated. The influence of terms with $m = n = 1$ and $m = 2$, $n = 1$ on electronic spectra has been studied in detail for (hexafluoroacetylacetonato)dimethylgold(III) and values of k_c have been determined from fits to experimental spectra.[38] In our model, both the values of m and n and the magnitude of k_c for each coupling term are defined by the spectroscopic parameters in Tables 1 and 2. The coupling between the coordinates $Q_{M=O}$ and Q_{M-L} is an effect of the interacting electronic states of the title compounds.

We use the time-dependent theory of emission spectroscopy[39,40] for our calculations. This approach allows us to calculate spectra for all models within the same framework. The emission spectrum is given by:

$$I_{lum}(\omega) = C\omega^3 \int_{-\infty}^{+\infty} e^{i\omega t}\{\langle\phi|\phi(t)\rangle e^{-\Gamma^2 t^2 + iE_{00}/\hbar t}\}\, dt \qquad (8)$$

ϕ represents the nuclear wave function of the molecule at $t = 0$ on the ground-state potential surface. The most important ingredient determining the vibronic structure and band shape of the luminescence spectrum is the autocorrelation function $\langle\phi|\phi(t)\rangle$ of the wave packet evolving on the ground-state potential surface. Γ is a phenomenological damping factor adjusted to reproduce the resolution of the experimental spectra and E_{00} is the energy of the electronic origin, given in Table 1 for the title compounds. We assume a harmonic surface for the emitting state and make the Condon approximation for all calculations, using a transition dipole that is independent of $Q_{M=O}$ and Q_{M-L}. This assumption is justified because progressions built on vibronic origins are experimentally observed to have intensity distributions identical with those on pure

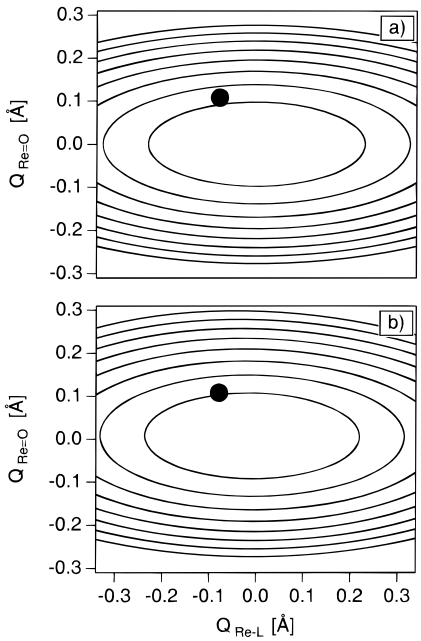

Figure 4. Ground-state potential energy surface for *trans*-ReO_2(1-vinylimidazole)$_4^+$: (a) diabatic surface and (b) lowest adiabatic surface obtained from eq 1. The dots indicate the position of the emitting state potential minimum. The energy minimum of both contour diagrams is at 0 cm^{-1} and contour lines are shown at intervals of 2000 cm^{-1}.

(38) Wexler, D.; Zink, J. I. *J. Phys. Chem.* **1993**, *97*, 4903.

(39) Heller, E. J. *J. Chem. Phys.* **1975**, *62*, 1544.

(40) Zink, J. I.; Kim Shin, K.-S. In *Advances in Photochemistry*; Volman, D. H., Hammond, G. S., Neckers, D. C., Eds.; John Wiley: New York, 1991; Vol. 16, p 119.

electronic origins in many transition metal compounds with inversion symmetry.[41] The crystal structures of the ethylenediamine and oxalate complexes have a center of inversion at the metal site.[21,24,28] The luminescence spectra of *trans*-$ReO_2(tmen)_2^+$, *trans*-$ReO_2(en)_2^+$, *trans*-$OsO_2(en)_2^{2+}$, and *trans*-$OsO_2(ox)_2^{2-}$ are therefore superpositions of spectra built on vibronic origins that are too close in energy to be resolved in our experiments. The crystallographic point group symmetry of the *trans*-ReO_2(R-imidazole)$_4^+$ compounds does not retain the inversion center,[26] relaxing the parity selection rule and leading to a weakly allowed electronic transition in addition to progressions built on vibronic origins. This superposition is a likely cause of the limited resolution of the luminescence spectra, in contrast to the allowed oxo → metal charge-transfer absorption bands, where line widths of less than 20 cm^{-1} are observed for some of the title compounds.[20,29,33]

The time-dependent wave function $\phi(t)$ in eq 8 is calculated on a two-dimensional grid representing the ground-state potential surface with the split operator algorithm developed by Feit and Fleck:[42]

$$\phi(t + \Delta t) = e^{(i\Delta t/4M)\nabla^2} e^{-i\Delta t V} e^{(i\Delta t/4M)\nabla^2} \phi(t) + O[(\Delta t^3)] \quad (9)$$

Equations 8 and 9 allow us to calculate the autocorrelation function $\langle\phi|\phi(t)\rangle$ and the luminescence spectrum.

Luminescence Spectra from Harmonic Potential Energy Surfaces. Harmonic potentials provide an excellent starting point for the analysis of vibronic structure in electronic spectra of transition metal compounds and have been extensively used to calculate spectra for a large number of transition metal complexes and organometallic molecules.[40,43] We use them first to calculate the resolved luminescence spectra for the *trans*-dioxo complexes of rhenium(V) shown in Figure 1. The vibrational energies of the ground and emitting state potentials are determined from luminescence, Raman, and absorption spectra and are summarized in Table 1. A calculated luminescence spectrum based on harmonic surfaces is given in the literature for *trans*-$ReO_2(py)_4^+$ and is in perfect agreement with the experimental spectrum.[6] The positions of the minima along the normal coordinates are the only adjustable parameters and absolute values of 0.07 and 0.03 Å are obtained for the rhenium−oxo and rhenium−pyridine bond length changes, respectively.[6] The corresponding changes along the normal coordinates $\Delta Q_{Re=O}$ and ΔQ_{Re-L} are 0.10 and 0.06 Å, respectively. The literature luminescence spectrum of *trans*-$OsO_2(CN)_4^{2-}$ shows weakly resolved vibronic structure with a separation between peaks corresponding to the Raman active Os═O mode.[9,20] We estimate a value of 0.10 Å for $\Delta Q_{Os=O}$ from the literature spectra, very similar to the values reported in Table 2 for the two *trans*-dioxo complexes of osmium(VI) in Figure 2. Calculations based on harmonic potentials are shown in Figures 5, 7, and 8 for all title compounds. The parameters used for the calculations are summarized in Table 2.

There are two important discrepancies between experimental spectra and calculations based on harmonic surfaces. Both arise from the terms coupling the coordinates $Q_{M=O}$ and Q_{M-L} as a consequence of the interactions between the ground and excited electronic states. The first difference is indicated by the sloping lines on top of the experimental and calculated spectra in Figures 5 and 7. Each cluster of bands forming the main progression in *trans*-$ReO_2(vi\text{-}im)_4^+$ and *trans*-$ReO_2(en)_2^+$ has a different shape from its neighbors, leading to the nonreplica patterns[38] emphasized by the sloping lines. This variation is more pronounced for molecules which emit at low energies, such as the ethylenediamine and 1-vinylimidazole compounds in Figure 1. In contrast, it is weak or negligible for complexes which emit at higher energies, such as the tetramethylethylenediamine complex in Figure 1 or the pyridine complex, where the harmonic model is in excellent agreement with the experimental spectra.[5,6] The second important difference concerns the shape of the luminescence spectrum calculated for *trans*-$OsO_2(ox)_2^{2-}$, which differs from the Poisson band shape calculated for a harmonic ground-state surface. Two mono-oxo complexes of rhenium(V) with near-infrared luminescence bands also show unusual band shapes.[44] These envelopes will be analyzed in the final section of the discussion.

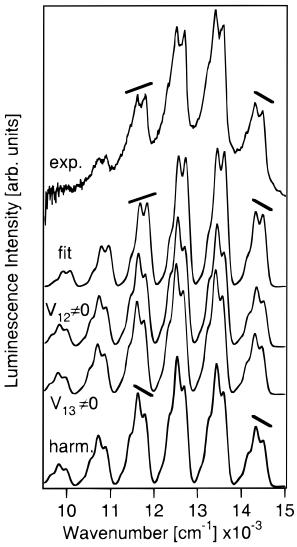

Figure 5. Comparison of calculated luminescence spectra for *trans*-$ReO_2(1\text{-vinylimidazole})_4^+$. Top to bottom are the experimental spectrum, the spectrum resulting from the best fit to eq 1 with the potential in Figure 4b, the spectrum with $V_{12} \neq 0$, the spectrum with $V_{13} \neq 0$, and the spectrum calculated for the harmonic ground-state surface in Figure 4a.

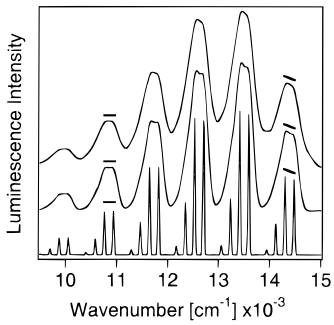

Figure 6. Effect of resolution on the vibronic structure of the calculated luminescence spectrum of *trans*-$ReO_2(1\text{-vinylimidazole})_4^+$. The bottom and middle spectra are calculated from the same model as the best fit in Figure 5, but with line width parameters Γ (eq 8) of 10 and 60 cm^{-1}, respectively. The top spectrum is a weighted superposition of 11 best fit spectra displaced along the abscissa to simulate the effect of inhomogeneous broadening.

Resolved Vibronic Structure for *trans*-Dioxo Complexes of Rhenium(V). The vibronic structure observed for *trans*-

(41) Flint, C. D. *Coord. Chem. Rev.* **1974**, *14*, 47.
(42) Feit, M. D.; Fleck, J. A, Jr.; Steiger, A. *J. Comput. Phys.* **1982**, *47*, 412.
(43) Brunold, T.; Güdel, H. U. In *Inorganic Electronic Structure and Spectroscopy*; Solomon, E. I., Lever, A. B. P., Eds.; John Wiley: New York, 1999; Vol. I, p 259.
(44) Oetliker, U.; Savoie, C.; Stanislas, S.; Reber, C.; Connac, F.; Beauchamp, A. L.; Loiseau, F.; Dartiguenave, M. *Chem. Commun.* **1998**, 657.

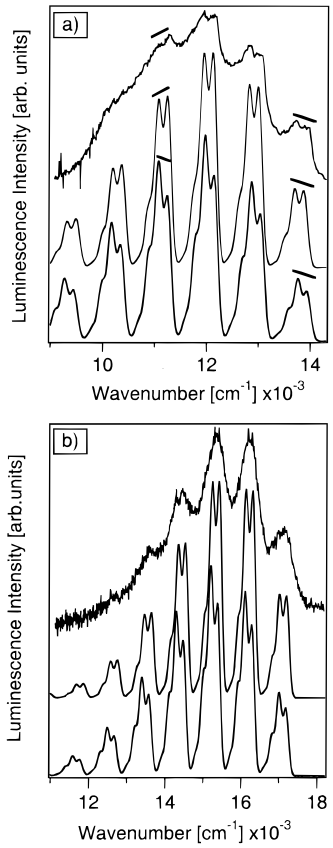

Figure 7. Calculated and experimental luminescence spectra of (a) *trans*-$ReO_2(en)_2^+$ and (b) *trans*-$ReO_2(tmen)_2^+$. The top trace in both sections is the experimental spectrum, followed by the spectrum calculated from the lowest adiabatic potential in eq 1 and the spectrum calculated from harmonic potential surfaces.

$ReO_2L_n^+$ ($n = 2, 4$) complexes with low-energy emission is influenced by all three A_{1g} electronic states defined in eq 1. We use in the following the model outlined in the first section of the discussion to rationalize the spectra observed for the rhenium(V) complexes in Figure 1. We have previously reported a phenomenological model that was sufficient to quantitatively describe the nonreplica vibronic pattern of *one* complex, *trans*-ReO_2(1-methylimidazole)$_4^+$, by adding a single $k_cQ_{Re=O}{}^2Q_{Re-L}$ term coupling the two normal modes to the harmonic ground-state potential and fitting the adjustable parameter k_c.[45] This coupling constant was found to be smaller by approximately 2 orders of magnitude than the rhenium−oxo and rhenium−L vibrational energies. The phenomenological model does not allow us to rationalize the presence or absence of nonreplica patterns in the luminescence spectra of the closely related rhenium complexes presented here and reported previously,[32] but we found that the adjustable parameter k_c is largest for low-energy luminescence spectra, a qualitative correlation that has inspired us to develop the model described here.

Figure 5 shows a detailed comparison between spectra calculated from several models and the experimental spectrum of *trans*-ReO_2(vi-im)$_4^+$ (top trace). The spectrum corresponding to the full three-level model given in eq 1 and Figures 3 and 4 provides the best overall fit and is shown directly below the experimental spectrum. The harmonic spectrum (bottom) does not reproduce the variation of the vibronic structure along the main progression at all, because all interactions with excited states are neglected. This is obvious from a comparison of the sloping lines above the first and fourth members of the main progression in both the experimental and calculated spectra shown in Figure 5. The spectra calculated from models with only two coupled levels are shown as the third and fourth traces in Figure 5 and do not lead to a variation of the shape of each member of the main progression that matches the experiment. Even increasing the only remaining coupling constant V_{12} or V_{13} in these models does not result in calculated spectra that show as good an agreement with experiment as the spectrum from the full calculation with eq 1. The effect of two excited states with different potential energy minima along Q_i on the ground-state potential surface appears to be essential. The comparison in Figure 5 shows that the full model in eq 1 has to be used to quantitatively rationalize the observed vibronic structure.

Figure 6 illustrates the influence of the vibronic line width and inhomogeneous broadening on the calculated luminescence spectrum of *trans*-ReO_2(vi-im)$_4^+$. The bottom and middle traces are calculated with the same model as the best fit spectrum shown in Figure 5, but with damping factors Γ of 10 and 60 cm^{-1} for the high- and low-resolution spectra, respectively. These calculated spectra show nonreplica patterns very similar to the best fit in Figure 5, indicating that this effect does not depend on the bandwidth of individual vibronic lines. The resolution and background of the experimental luminescence spectra are most likely determined by inhomogeneous broadening. The top spectrum in Figure 6 illustrates the result of a weighted addition of spectra displaced along the abscissa axis, shown as the sum of the best fit spectrum from Figure 5 (weight 30%) and best fit spectra displaced by $\pm$70 cm^{-1} (15% each), $\pm$140 cm^{-1} (7% each), $\pm$210 cm^{-1} (4% each), $\pm$280 cm^{-1} (4% each), and $\pm$350 cm^{-1} (4% each). This calculated spectrum provides a good reproduction of the background intensity between the members of the main progression in the experimental spectrum in Figure 5 and it retains the vibronic intensity distribution of the best fit calculation. The comparison of all spectra indicates that the intensity variations along the main progression are not significantly affected by line broadening or by an unresolved background.

The lowest adiabatic surface is sufficient to calculate spectra because only negligible wave packet amplitude extends to the region of the avoided crossing between the potential surfaces illustrated in Figure 3. The energy difference between the ground-state minimum and the initial position of the wave packet, indicated by the black dots in Figure 4, is 2470 cm^{-1} for the harmonic surface in Figure 4a and 2030 cm^{-1} for the potential in Figure 4b. The difference of 440 cm^{-1} between these two energies is due to coupling between the ground and excited electronic states, as derived with our model from the low-temperature luminescence spectra. The difference is obvious from Figure 4, where the dot indicating the emitting state minimum is outside the innermost (2000 cm^{-1}) contour line for the harmonic potential in Figure 4a, but intersects this contour line for the potential including coupling in Figure 4b. The terms coupling normal coordinates cause wave packet dynamics on the potential energy surface in Figure 4b that can no longer be separated into independent $Q_{M=O}$ and Q_{M-L} dynamics, as has been illustrated in detail for a two-dimensional potential surface $V(Q_1,Q_2)$ with a single $k_cQ_1{}^2Q_2$ coupling term.[46]

The same approach was applied to the ethylenediamine and tetramethylethylenediamine compounds and leads to satisfactory spectra calculated with eq 1, as illustrated in Figure 7. The calculated spectra show the importance of the energy difference

(45) Savoie, C.; Reber, C.; Bélanger, S.; Beauchamp, A. L. *Inorg. Chem.* **1995**, *34*, 3851.

(46) Tannor, D. J. *J. Phys. Chem.* **1993**, *97*, 4903.

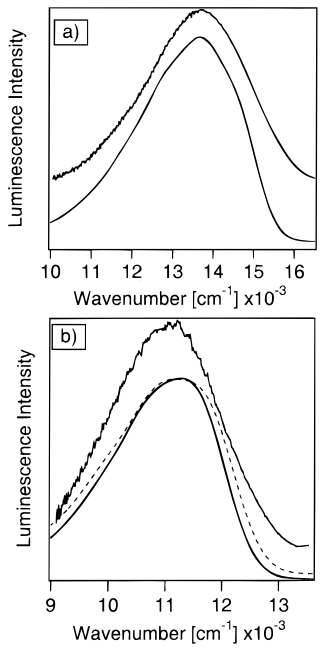

Figure 8. Calculated and experimental luminescence spectra of (a) *trans*-$OsO_2(en)_2^{2+}$ and (b) *trans*-$OsO_2(ox)_2^{2-}$. The top traces in both sections denote the experimental spectrum. The calculated spectrum of *trans*-$OsO_2(en)_2^{2+}$ is obtained from a one-dimensional harmonic potential surface and shown as the bottom trace in part a. The calculated spectrum of *trans*-$OsO_2(ox)_2^{2-}$ based on harmonic potential energy surfaces is shown as a dotted line in part b. The spectrum calculated from a model including coupling between two potential surfaces is given as a solid line (bottom trace in part b).

between the electronic states: the effect is easily seen in the experimental luminescence spectrum of *trans*-$ReO_2(en)_2^+$, but it is much less obvious for the tetramethylethylenediamine complex. The parameters used for the two complexes are very similar, with the exception of the interelectronic repulsion parameter, K_{xy}, which is significantly larger for the ethylenediamine complex.

The values determined for ΔQ_i in Table 2 are very similar for the three rhenium complexes, but the detailed vibronic structure of their luminescence spectra varies and the spectra do not have the same overall bandwidths: the spectrum of the ethylenediamine complex is narrower than the spectrum of *trans*-$ReO_2(tmen)_2^+$, which has its maximum at higher energy. The same trend is observed for *trans*-dioxo complexes of osmium(VI) and discussed in the following section. The model in eq 1 involving three coupled electronic states therefore provides a complete and quantitative explanation for the observed spectroscopic effects.

Band Shapes of *trans*-Dioxo Complexes of Osmium(VI). The unresolved band shapes of the *trans*-OsO_2L_2 complexes in Figure 2 also show distinct evidence for interacting ground and excited electronic states. We calculate spectra from a simplified model including only one normal coordinate, the osmium−oxo mode $Q_{Os=O}$. The spectrum of *trans*-$OsO_2(en)_2^{2+}$ resulting from a harmonic ground state potential surface is shown in Figure 8a. Both the shape of the calculated band and its width are in very good agreement with the experimental spectrum. The only adjustable parameter is $\Delta Q_{Os=O}$, reported in Table 2. Our value of 0.10 Å is within the range of literature values given as 0.10−0.12 Å for *trans*-$OsO_2(CN)_4^{2-}$.[20]

The spectrum of *trans*-$OsO_2(ox)_2^{2-}$ is compared to the calculation based on a harmonic potential energy surface in Figure 8b (dotted line). The high-energy onset of the calculated spectrum is steeper than observed experimentally and the low-energy decrease of the calculated intensity occurs slower than in the experimental spectrum. It is not possible to simultaneously remove both discrepancies with a harmonic ground-state surface. The experimental band shapes at 10 and 80 K are very similar and differ from a Poisson envelope. The constant luminescence lifetimes across the band shape indicate that the envelope is not due to two or more overlapping harmonic spectra. The value of 0.085 Å for $\Delta Q_{Os=O}$ obtained from the fit is smallest among the values in Table 2, possibly related to the osmium−oxo bond length of *trans*-$OsO_2(ox)_2^{2-}$ which is 0.03 Å shorter than in *trans*-$OsO_2(en)_2^{2+}$ [21,28] or due to the competition between metal−oxo and metal−oxalate π bonding.[24,34]

We improve our model by including interactions between the ground state and the lowest energy excited state, involving a single coupling constant V_{12}. The energy of this excited state is obtained from the absorption and luminescence spectra and given in Table 2. The calculated spectrum shown as a solid line in Figure 8b (bottom trace) is obtained from the upper left 2×2 section of the matrix in eq 1 by adjusting V_{12}. Increasing its value leads to a narrower calculated band shape with a steeper decrease of the intensity at low energies and improves the agreement with the experiment, as shown in Figure 8b. A qualitatively similar change in the band envelope as a consequence of coupling is observed for the low-energy emission of the rhenium compounds in Figures 5 and 7b. The remaining discrepancies between experimental and calculated band shapes are most likely due to the limitation to only one excited state interacting with the ground state of the osmium(VI) complexes, unlike the rhenium compounds, where the full model with two excited states in eq 1 was used. The unresolved luminescence spectra and the limited crystal field absorption data of the osmium(VI) complexes do not provide sufficient experimental information to define all the parameters necessary for a model involving three electronic states.

The reason for the narrowing of the band envelope is evident from a comparison of the autocorrelation functions $\langle\phi|\phi(t)\rangle$ in eq 8 obtained for harmonic ground-state potentials and for the surfaces including coupling to excited states. At the initial position of the wave packet, the harmonic ground-state potential of each title compound has a steeper slope than the lowest adiabatic surface arising from the coupled model, as illustrated for *trans*-$ReO_2(vi\text{-}im)_4^+$ in Figures 3 and 4. The slope of the surface region explored by the wave packet at short times determines the initial decrease of the autocorrelation function. A rapid decrease is calculated from harmonic surfaces as illustrated by the dotted lines in Figures 9a and 9b for *trans*-$OsO_2(ox)_2^{2-}$ and *trans*-$ReO_2(en)_2^+$, respectively. These autocorrelations lead to a broad Poisson band envelope.[39,40] The adiabatic surfaces are flattened in the region below the emitting state minimum and we calculate a slower decrease of the autocorrelation, shown as solid lines in Figures 9a and 9b, leading to the narrower band envelopes and deviations from a Poisson band shape illustrated for *trans*-$OsO_2(ox)_2^{2-}$ in Figure 8b and for *trans*-$ReO_2(en)_2^+$ in Figure 7b.

The autocorrelation functions for the two calculated spectra of *trans*-$ReO_2(en)_2^+$ in Figure 7a are compared over a longer time period in Figure 9c. Autocorrelation maxima occur every 37.9 fs on the harmonic ground-state surface, shown as a dotted line in Figure 9c. This time interval leads to a constant energy separation of 880 cm^{-1} between the calculated maxima of the main progression. It is obvious that the recurrences occur later in time for the autocorrelation calculated with the adiabatic surface including coupling (solid line in Figure 9c) than for the

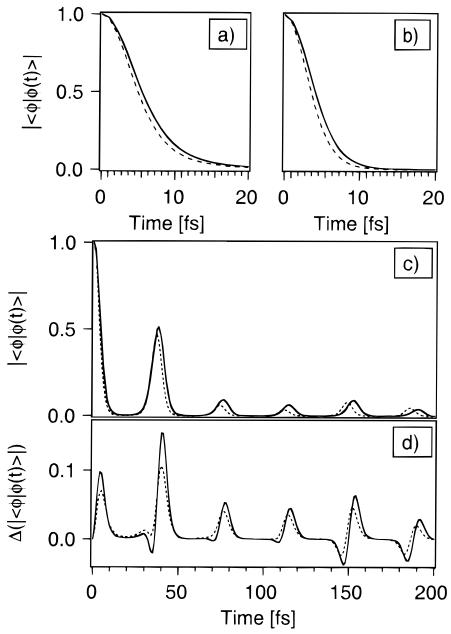

Figure 9. (a) Absolute autocorrelation function for *trans*-$OsO_2(ox)_2^{2-}$. The solid line denotes the autocorrelation for the adiabatic potential with nonzero coupling, the dotted line shows the autocorrelation for a harmonic potential. (b) Absolute autocorrelation function at short times for *trans*-$ReO_2(en)_2^+$. (c) Autocorrelation for *trans*-$ReO_2(en)_2^+$. (d) Difference between coupled and uncoupled autocorrelations for *trans*-$ReO_2(en)_2^+$ (solid line) and *trans*-$ReO_2(tmen)_2^+$ (dotted line).

autocorrelation obtained with the harmonic surface. The difference is 1.0 fs for the first recurrence, which corresponds to an energy interval of 857 cm^{-1}, and increases to 4.6 fs for the fifth peak in Figure 9c. These longer times lead to maxima of the main progression which occur at slightly lower energy than those of the spectrum resulting from a harmonic surface. The time differences between maxima of the autocorrelation shown as a solid line in Figure 9c are not constant for the adiabatic potential defined in eq 1 and lead to energy differences between members of the main progression that vary across the spectrum. These properties of the autocorrelation function cause the distinct intensity variations indicated by the sloping lines in Figures 5 and 7: the maximum of the first member of the main progression occurs later in its series of low-frequency peaks than for the fourth member of the main progression, which has its maximum intensity at the beginning of its cluster of low-frequency bands. The nonreplica pattern is clearly illustrated by the autocorrelation recurrences, which occur at longer times on the potential surface obtained from the full model in eq 1, illustrated for one compound in Figure 4b. Figure 9d illustrates the differences between autocorrelations from potentials including coupling to excited states and harmonic surfaces for *trans*-$ReO_2(en)_2^+$ (solid line) and *trans*-$ReO_2(tmen)_2^+$ (dotted line). The initial positive difference leads to the narrower band envelope and the shift of the autocorrelation recurrences causes the characteristic negative and positive autocorrelation differences at each recurrence. The comparison in Figure 9d shows that similar effects are observed for both compounds, but that they are much stronger for the complex with the lower energy emission, represented by the solid line in Figure 9d, again illustrating the influence of the excited electronic states on the ground-state potential energy surface. The model defined in eq 1 rationalizes the vibronic structure and luminescence band shapes for many $5d^2$ configured *trans*-dioxo compounds and gives a quantitative description of the ground-state potential energy surfaces for the title compounds.

Conclusion

The detailed comparison of luminescence spectra of *trans*-dioxo complexes allows us to determine the influence of excited electronic states on the ground-state potential energy surface. The resolved vibronic structure in luminescence spectra can be used to calculate this effect, but even the shape of unresolved band envelopes provides experimental evidence for coupling between the electronic ground and excited states.

Acknowledgment. This work was made possible by grants from the Natural Sciences and Engineering Research Council (Canada). We acknowledge contributions from Sandrine Stanislas, Andreea Vuica, Steve Masson, and Thierry Wamser.

JA993305Q